Strong Electron-Electron-Nuclei Correlations in Two-Photon Double Ionization of H_2

Kilian Arteaga,[1,2] Johannes Feist,[3,4] Denis Jelovina,[1,†] Fernando Martín,[1,2] and Alicia Palacios[1,4,5,*]

[1]*Departamento de Química, Módulo 13, Universidad Autónoma de Madrid (UAM), 28049 Madrid, Spain*

[2]*Instituto Madrileño de Estudios Avanzados en Nanociencia (IMDEA-Nanociencia), Cantoblanco, 28049 Madrid, Spain*

[3]*Departamento de Física Teórica de la Materia Condensada, UAM, 28049 Madrid, Spain*

[4]*Condensed Matter Physics Center (IFIMAC), UAM, 28049 Madrid, Spain*

[5]*Institute for Advanced Research in Chemical Sciences (IAdChem), UAM, 28049 Madrid, Spain*

(Received 25 April 2024; accepted 26 July 2024; published 17 September 2024)

Two-photon double ionization is a paradigmatic example of how electron correlation manifests. In molecular targets, its coupling with the slower nuclear motion introduces an additional complication and induces electron-electron-nuclei correlations. Experimentally, momentum-coincident measurements can provide a complete kinematical image of the molecular full Coulomb breakup. Previous theoretical studies have described this process by ignoring nuclear motion and the subsequent Coulomb explosion of the dication. Here we show, by means of a full-dimensional treatment of two-photon double ionization of the H_2 molecule, that nuclear motion plays a decisive role even for pulses as short as 1.5 fs, a time during which the nuclei are not expected to move significantly. We find strong correlations between nuclear and electronic degrees of freedom, giving access to different electronic processes as a function of nuclear kinetic energy. In particular, we observe unexpectedly strong back-to-back asymmetry in the photoelectron angular distributions, as well as novel interferences resulting from the coherent contributions from two-photon sequential absorption paths via different molecular cationic states.

DOI: 10.1103/PhysRevLett.133.123201

The rapid development of quantum technologies has revitalized the interest in quantum entanglement in many-body systems [1]. In this context, double ionization is a paradigmatic process for probing both electron interaction and entanglement, with the additional complication of electron-nuclear quantum entanglement in the case of molecules. Even in the helium atom, decades of work and the advent of the cold target recoil ion momentum spectroscopy were required to reach a consensus on a quantitative estimation of the single-to-double photoionization ratio under single-photon absorption (see [2,3] and references therein). The next milestone was the experimental quantification of two-photon double ionization, which became possible with the availability of intense soft-x-ray pulses from high harmonic generation [4] and free electron lasers (FELs) [5]. After those first experiments, an accurate theoretical description was soon achieved [6–10], showing an intricate interplay between sequential and nonsequential emission pathways leaving its signature in the angularly resolved photoelectron distributions [6–10]. The sequential process corresponds to two on-shell (energy-conserving) photon absorptions, first in the neutral and then in the cation, while the nonsequential one describes the almost simultaneous absorption of two photons where each interaction can be off shell (i.e., not fulfilling energy conservation) as long as the total process is on shell. Efforts are now focused to rationalize correlation effects in sequential versus nonsequential double ionization in few-electron atoms [11], where the electrons can be emitted from different shells, and in molecular targets, where the entangled nuclei bring into play a new timescale. In the latter, a possible delay between photon absorptions permits nuclear motion to occur, leading to the involvement of a wider range of geometries compared to single-photon absorption.

A complete kinematical reconstruction of the full Coulomb breakup of molecules, accounting for up to five charged ions in coincidence, has been experimentally achieved at FELs [12–17]. However, we are still far from a complete dynamical characterization of the process even for the simplest case, the hydrogen molecule [18,19], which calls for new theoretical methods to describe the laser-induced dynamics of four interacting charged particles. The most accurate theoretical predictions for multiphoton double ionization performed in H_2 up to date have employed the fixed-nuclei approximation (FNA) to evaluate energy and angularly resolved photoelectron spectra [20–27]. These works already discussed molecular orientation and two-center effects, obviously absent in its atomic analog [20,26,28]. However, a full-dimensional description including nuclear motion has remained out of reach until now due to the presence of the so-called exponential wall in

*Contact author: alicia.palacios@uam.es

†Present address: Computing Systems Laboratory, Huawei German Research Center, Zurich, Switzerland.

computational effort as the number of degrees of freedom is increased. In this Letter, we work at the limit of this wall and perform accurate full-dimensional calculations for the description of the four-body Coulomb breakup ($H^+ + H^+ + e^- + e^-$) of H_2 upon two-photon absorption from an attosecond extreme UV pulse (see Appendix for details). We examine how the nuclear degrees of freedom affect the photoelectron spectra and the correlation between the fragments at different photon energies and present an analysis of the angularly resolved photoelectron emission, revealing the signature of interferences between distinct sequential two-photon absorption paths.

We represent the total wave function $\Psi(\mathbf{r_1}, \mathbf{r_2}, \mathbf{R})$ using coupled spherical harmonics for the angular variables and the finite element method-discrete variable representation (FEM-DVR) for the radial variables [6–9,29–33]. We solve the time-dependent Schrödinger equation using this basis set in the presence of an external field. To enable direct comparison with existing studies within FNA, we employ a cosine-squared 30 eV laser pulse with a total duration of 1378 attoseconds (as) and an intensity of 10^{14} W/cm^2 [21–23,27] and additionally perform simulations for a 37.5 eV pulse. The energetics for each case are shown in Fig. 1, including a discussion of the different single and double ionization potentials.

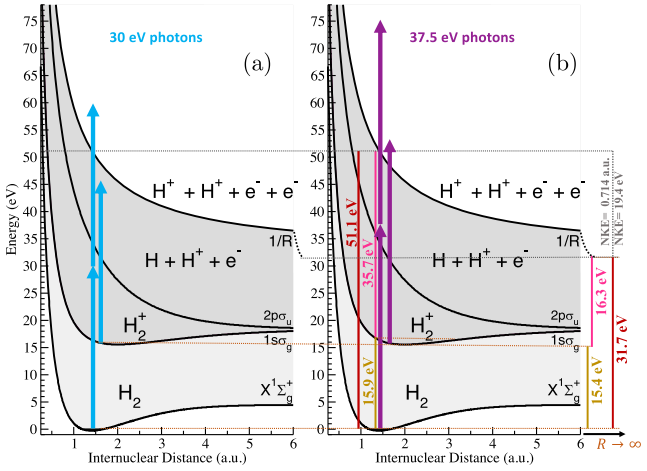

FIG. 1. Energy diagrams for two-photon double ionization of H_2 for (a) 30 eV and (b) 37.5 eV photons. The vertical double ionization potential (DIP_v) for H_2 at its equilibrium distance $R_{eq} = 1.4$ a.u. is $DIP_v = 51.1$ eV. The single IPs of H_2 and H_2^+ at the same geometry are 15.9 and 35.7 eV, respectively. Therefore, when assuming frozen nuclei, nonsequential double ionization opens at ≈25.6 eV (51.1/2 eV), while the sequential emission requires at least 35.7 eV, and the nuclear kinetic energy (NKE) is always given by $1/R_{eq} = 19.4$ eV. Since the nuclei actually move, one should consider the adiabatic ionization potentials that are significantly lower. The adiabatic double ionization potential DIP_a is 31.7 eV, and the single ionization ones are 15.4 eV for the neutral and 16.3 eV for the cation via the $H_2^+(1s\sigma_g)$. Consequently, a sequential emission of electrons is energetically possible above 16.3 eV.

Figures 2(a) and 2(b) show the two-photon double ionization probability density for central pulse frequencies of 30 and 37.5 eV, respectively, through photoion-photoelectron coincidence maps as a function of the nuclear kinetic energy NKE (y axis) and electron energy E_e (x axis) for one of the electrons, integrating over the second one. These coincidence maps already display several crucial features of the two-photon process that are purely due to nuclear motion. Within the FNA, the sequential double ionization process only opens for photon energies above 35.7 eV, which is the IP of H_2^+ at the equilibrium distance $R_{eq} = 1.4$ a.u. (see Fig. 1). In contrast, when nuclear motion is allowed, the rapid decrease of the adiabatic ionization potentials with the internuclear distance due to the purely Coulombic nature of the H_2^{++} potential allows for the sequential process to open at much lower photon energies as the molecular ion vibrates and reaches larger internuclear separations; for a photon energy of 30 eV, this process opens at $R = 1.9$ a.u. within the adiabatic picture, at the edge of the Franck-Condon region. For low nuclear energies, we indeed observe the double-peak structure typical of sequential electron emission [e.g., along the lower dashed white line in Fig. 2(a)], in contrast to the smooth distribution at higher NKEs (along the upper dashed white line). For low NKEs, the lower peak always

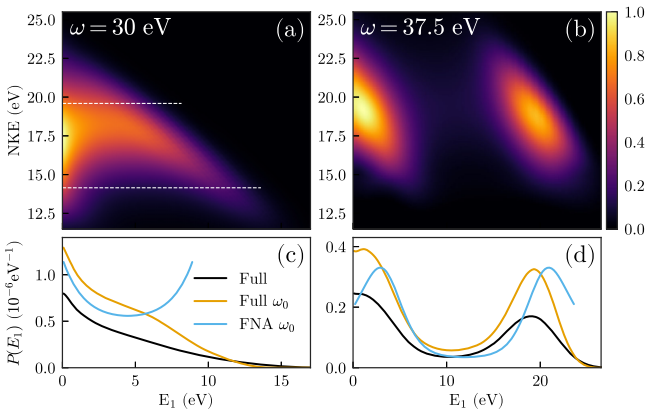

FIG. 2. (a),(b) Double ionization probability density as a function of electronic (x axis) and nuclear (y axis) kinetic energy (NKE), integrated over the pulse bandwidth and energy of the second electron, for central pulse frequencies of (a) $\omega_0 = 30$ eV and (b) $\omega_0 = 37.5$ eV. The color scale is normalized to the maximum value for each plot, given by (a) $P_{max} \approx 1.14 \times 10^{-7}$ eV^{-2} and (b) $P_{max} \approx 4.61 \times 10^{-8}$ eV^{-2}. White dashed horizontal lines in (a) indicate the cuts discussed in the text for representative NKE values. (c),(d) Same probabilities as (a),(b) plotted as a function of energy for electron 1 (E_1) and integrated over NKE are plotted as black lines (given in units of 10^{-6} eV^{-1}). Orange and blue lines correspond to the photoelectron distribution at a given final energy (at the peak of each pulse, $E_{tot} = E_0 + 2\omega_0$) for the full and the FNA simulations, respectively (these have been multiplied by 10 eV for comparison, which is equivalent to the y axis being given in units of 10^{-7} eV^{-2}).

appears at low electron energies, while the higher peak is determined by energy conservation dictating that $E_1 + E_2 + \mathrm{NKE} \approx 2\omega_L - \mathrm{DIP}_a$ (within the bandwidth of the pulse). This indicates that the yield is dominated by processes where the sequential process is just barely energetically allowed. The efficiency of the electronic sequential process, the cross section of which diverges for infinitely long pulses [9], is then responsible for the large yield at much lower NKEs than would be expected within the FNA, where the NKE is given by $1/R_{\mathrm{eq}} \simeq 0.714$ a.u. (19.4 eV) as follows from the reflection approximation.

For the 37.5 eV pulse, where the sequential process is enabled even within the FNA (see violet arrows in Fig. 1), the electron-nuclear coincidence energy map, in Fig. 2(b), shows two clearly distinct peaks for any value of the NKE. These peaks have a width in total energy determined by the pulse energy bandwidth and are tilted due to the smaller available energy to be shared by the electrons as the energy of the nuclei increases.

Figures 2(c) and 2(d) show the same probabilities integrated over NKE (black full lines) and, additionally, the ionization probability density for a fixed total energy $E_f = E_0 + 2\omega_L$ corresponding to two-photon absorption at the central pulse frequency (orange) and the same quantity within the fixed-nuclei approximation (blue). For the 30 eV pulse, Fig. 2(c), there is a marked difference between the FNA and the full simulation: While the former resembles atomic nonsequential two-photon absorption, i.e., an almost symmetric distribution and a smile-type shape [6–9], the inclusion of nuclear motion leads to a redistribution of energy between nuclei and electrons, translating into broken symmetry in electron energy and a significant increase of probability for less energetic electrons. For the 37.5 eV pulse, Fig. 2(d), the same effect is present, but is less prominent due to the dominance of the sequential process.

We now turn to the (joint) angular distributions of the photoelectrons, where correlation effects manifest even more clearly. Electron emission by a sequential two-photon process is expected to be less correlated than the nonsequential case, as previously shown in atomic targets [6–9,34]. In the simplest configuration interaction picture, with an expansion over atomiclike orbitals which becomes accurate in the united-atom limit, the sequential process corresponds to the absorption of one photon by each electron in the dominant $1s1s$ configuration representing the ground state, which would lead to the final configuration $\epsilon p \epsilon' p$ ($1s1s \rightarrow 1s\epsilon p \rightarrow \epsilon p \epsilon' p$), giving an uncorrelated cosine-squared angular distribution. For nonsequential emission, on the other hand, one expects a back-to-back emission of electrons since they are emitted simultaneously and their mutual Coulomb repulsion suppresses emission in the same direction. Figure 3 shows the molecular-frame photoelectron angular distributions for the 37.5 eV pulse

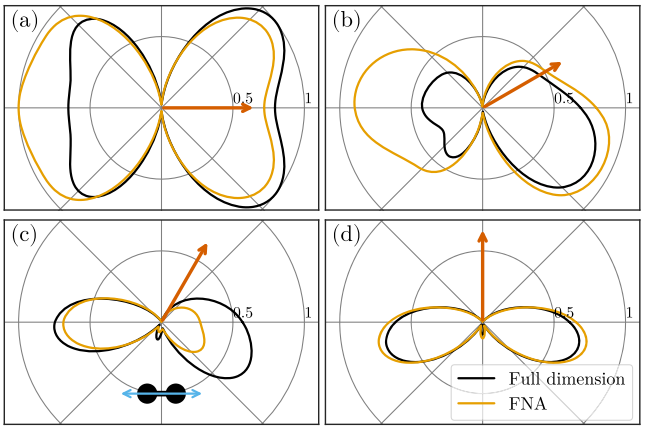

FIG. 3. Photoelectron angular distributions for the fast electron (with an energy of ≈23 eV) in double ionization for the 37.5 eV pulse. We compare the double ionization probability density (radial scale) obtained within fixed-nuclei approximation (orange line) with the full-dimensional simulations at a NKE of ≈19.4 eV (i.e., vertical transition). The dark orange arrow indicates the emission angle of the slow electron (≈1 eV) with respect to the light polarization direction, given by (a) 0°, (b) 30° (c) 60°, and (d) 90°. The angular distributions are normalized to their maximum value for easier comparison, corresponding to $P_{\mathrm{max}} \approx 1.12 \times 10^{-6}$ sr^{-2} eV^{-3} for the full-dimensional simulation and $P_{\mathrm{max}} \approx 7.76 \times 10^{-8}$ sr^{-2} eV^{-2} for the fixed-nuclei approximation.

polarized parallel to the molecular axis (blue double arrow), with results obtained in the full-dimensional simulation (black line) shown for an NKE of 19.4 eV, corresponding to a vertical transition for easy comparison with the FNA, and for electron ejection energies close to the sequential emission peaks, $E_1 \approx 23$, $E_2 \approx 1$ eV. The FNA results are shown for the same electronic energies (orange line). Each subplot shows the double ionization probability as a function of the emission angle of the fast electron and for a fixed angle of the slower electron indicated by the orange arrow. Because of the dominance of the sequential process, we find distributions resembling a cosine-squared shape, although clear deviations appear due to the electron-electron interaction and, more importantly, due to the loss of spherical symmetry in a molecule, which increases the contribution from higher angular momenta. The inclusion of nuclear motion enhances this effect due to contributions from larger internuclear distances in the dynamics.

The overall variation of electron correlation with the energy sharing of electrons and nuclear fragments is illustrated in Fig. 4. The insets show the photoelectron angular distributions for a given NKE [vertical transition with NKE ≈ 19.4 eV in Figs. 4(a) and 4(c) and NKE ≈ 14.15 eV in Figs. 4(b) and 4(d)]. The legend in the insets indicates the percentage of energy taken by the electron. Overall, we find that electron correlation is stronger in H_2 than in its atomic counterpart, He [6–9]: For 30 eV photon energy, insets of Figs. 4(a) and 4(b), the electrons are ejected back-to-back regardless of the energy sharing, even

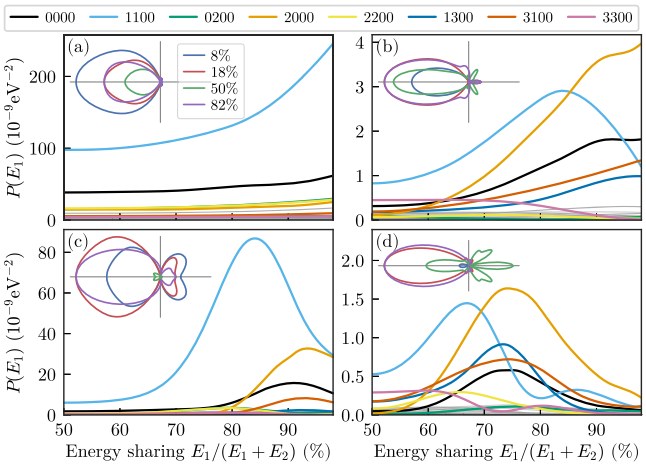

FIG. 4. Insets: photoelectron angular distributions (same conventions as in Fig. 3) for different energy sharings (given in the legends) for the fixed electron, which is fixed as in Fig. 3(a). (a)–(d) Contribution to the double ionization probability from each partial wave in the expansion, with the angular values (l_1, l_2, m_1, m_2) of both photoelectrons in the continua. The double ionization probabilities are plotted as a function of the energy sharing between electrons. Results (a),(b) for a 30 eV pulse and (c),(d) for a 37.5 eV pulse. (a),(c) Correspond to the case where protons are detected with an energy NKE ≈ 19.4 eV (vertical transition from the ground state). (b),(d) Correspond to NKE ≈ 14.15 eV (where the sequential emission of electrons is open for both cases).

at electron energies where the sequential process dominates [clear peaks in Figs. 2 and 4(b)]. Even for the lower NKE and electron energies at which the sequential peaks rise clearly in Figs. 2 and 4(b), the back-to-back emission remains. For the 37.5 eV pulse, insets of Figs. 4(c) and 4(d), we again observe a tendency to be emitted along the light polarization axis and in the opposite direction of the slow electron. Only when the electron escapes with a relatively large energy (92% or 82% of all the available energy), the probability to be emitted in the forward direction increases appreciably. Note that the almost pure back-to-back emission occurs already for electrons taking relatively large energies (50%, 60%, and 70%), with electron energy sharings that lead to a well-defined peak in Figs. 2(b) and 2(d). At equivalent absolute and relative electron energies, the He atom shows an almost totally uncorrelated behavior, with cosine-squared shapes in the angular distributions [6–9]. These results thus reveal that the multicenter character of the molecular potential introduces stronger correlation effects in the double photoelectron emission, which are further enhanced when accounting for nuclear motion.

To obtain a more complete picture, the main panels of Fig. 4 show the contributions of the different partial waves (angular momentum channels) to the double ionization as a function of the energy sharing of the electrons. The different angular contributions are labeled as l_1, l_2, m_1, m_2, such that, e.g., 1100 corresponds to both electrons being ejected with individual angular momenta $l = 1$ and $m = 0$. The angular distribution results from the coherent addition of these terms, therefore their relative weight provides rich information. We note that, due to the dipole selection rules, all configurations fulfill $M = m_1 + m_2 = 0$ and have Σ_g^+ total final symmetry. Figure 4(a) shows the results for the 30 eV pulse at a NKE within the Franck-Condon region from the ground state, i.e., when the electrons, at every energy sharing, are emitted after a nonsequential two-photon absorption process. The total available energy for electrons is thus 8.46 eV [$30 \times 2 - (1/R_{\mathrm{eq}}) - E_g$]. We observe that the largest contribution, as expected, is the 1100 (or $\varepsilon p \varepsilon' p$) channel coming from the dominant $1s1s$ contribution of the ground state. The second largest contribution, 0000, is compatible with emission from the second dominant configuration in the ground state ($2p2p$ type) [35]. An important observation from Fig. 4(a) is the almost independent variation of the double ionization probability for any partial wave as a function of the electron energy sharing, with only a slight increase at the most extreme energy sharing, as already explained, due to the expected larger contribution of the sequential process through the $1s\sigma_g$ state. For a lower NKE [14.15 eV in Fig. 4(b)], where the two electrons now share a total energy of 14.2 eV, we observe that the higher angular momenta come into play. For instance, at 50% of electron energy sharing, in addition to the dominant $\varepsilon p \varepsilon' p$ (1100) configuration, there is a significant contribution from $\varepsilon f \varepsilon' f$ (3300). In the Coulomb explosion curve ($1/R$), this NKE corresponds to an internuclear distance of $R \approx 1.9$ a.u., where the electronic state deviates from atomiclike (spherical) configurations and requires higher angular momenta to be described. Figure 4(b) captures the appearance of the sequential peaks due to nuclear motion. Since the IP from the $H_2^+(1s\sigma_g)$ cationic state significantly decreases with increasing R, it is now energetically possible to emit a second electron through a sequential transition.

For the 37.5 eV pulse [NKE of 19.4 in Fig. 4(c) and 14.15 eV in Fig. 4(d)], an interference of the two-photon sequential paths through the $H_2^+(1s\sigma_g)$ and the $H_2^+(2p\sigma_u)$ states emerges. These two channels lead to similar final electron energies, as the ionization potentials of the two channels are similar, but interchanged in order. At the equilibrium geometry, they are 15.9 and 35.7 eV through the $H_2^+(1s\sigma_g)$ state, and 34.23 and 16.9 eV through $H_2^+(2p\sigma_u)$. With a 37.5 eV photon, the first photoabsorption ionizes into the $H_2^+(2p\sigma_u)$ channel ($1s1s \rightarrow 2p\varepsilon s$), and the second into $\varepsilon d \varepsilon s$ (following the propensity rule). Therefore, we observe a significant increase in the contribution of the partial waves 2000 (and 0200). The sequential path through the $2p\sigma_u$ channel also affects other partial waves, in particular 1100, via electron-electron correlation, because the slow electrons emitted in the first photon absorption (at $E_1 = \omega - 34.23$ eV) are likely to be affected by the second, much faster electron at

$E_2 = \omega - 16.9$ eV. This shakeup process affects the relative contributions of each partial wave, but not significantly its variation with energy sharing. This implies that the observed interference structures are indeed due to two distinct two-photon paths reaching the same final state. We note that this path interference also appears in the fixed-nuclei approximation, but has not been discussed previously in the literature. For a given photon energy, different interference patterns arise depending on the NKE, as shown in Figs. 4(c) and 4(d). The energy of the first photoelectron, coming from the ground state, does not depend on NKE, but the energy of the second one strongly depends on the measured NKE, because the corresponding IPs strongly depend on R. Indeed, the IP for the $H_2^+(1s\sigma_g)$ decreases quickly with R, from 35.7 eV at $R = 1.4$ to 13.7 eV in the asymptotic limit. In contrast, the $H_2^+(2p\sigma_u)$ state is almost parallel to the double ionization potential. Consequently, the relative contributions of the sequential processes vary with the sharing of energy between the fragments. In a nutshell, the photoelectrons emitted with an ≈50% energy sharing are more likely produced by a sequential emission of electrons through the $1s\sigma_g$ cationic state, while for the most extreme electronic energy sharings, the probability of sequential emission is dominated by the $2p\sigma_u$ channel.

While the doubly excited states of the molecule, which appear as Rydberg series converging into each ionization threshold [36,37], are represented within our simulation, they do not play any role in the analysis. They are quasibound states (with both electrons excited) that only contribute to double ionization if the first photon simultaneously excites both electrons and the second photon simultaneously ionizes both of them, which only happens with very low probability. This observation has been confirmed in the He atom, where the contribution of doubly excited states can be extracted much more simply, confirming that they only play a role in two-photon single ionization and when using much longer and intense pulses. Therefore, in the two-photon double ionization of the molecule using attosecond pulses, the contribution of these states can be safely neglected.

To summarize, we have presented the first full-dimensional simulations of a multiphoton double ionization process in a molecule including nuclear motion. We find a significant impact of nuclear motion on the electron emission, increasing electron correlations both in the energetic and angular distributions compared to the atomic counterpart He. The strong correlation observed between all fragments in this four-body Coulomb breakup problem also implies that the commonly used fixed-nuclei approximation misses a significant part of the relevant physics. In particular, we find that the sequential process is opened at much lower photon energies, generating energy shifts in the energy-differential probabilities, and the angular distributions are significantly modified, showing unexpectedly highly correlated electron emission even when sequential double ionization dominates. Furthermore, we find nuclear-energy-dependent interferences from different intermediate cationic states in sequential double ionization. The present results demonstrate that nuclear motion effects are already visible even with ultrashort driving pulses of less than 2 fs duration, and they are expected to become even more prominent for longer pulses and especially for one- and two-color pump-probe schemes.

Acknowledgments—All calculations were performed at the Mare Nostrum Supercomputer of the Red Española de Supercomputación (BSC-RES MN4). Work is supported by the Spanish MICINN projects PID2021-125894NB-I00, PID2022-138288NB-C31, PID2022-138288NB-C32, CNS2023-145254, as well as PCD-IP3PCD026 from the PRICIT program of the Comunidad de Madrid. The authors also acknowledge support from the "Severo Ochoa" (SEV-2016-0686) and the "María de Maeztu" (CEX2023-001316-M) Programmes for Centers of Excellence in R&D.

[1] A. S. Maxwell, L. B. Madsen, and M. Lewenstein, Nat. Commun. **13**, 4706 (2022).
[2] R. Dörner *et al.*, Phys. Rev. Lett. **76**, 2654 (1996).
[3] H. Bräuning, R. Dörner, C. L. Cocke, M. H. Prior, B. Krässig, A. S. Kheifets, I. Bray, A. Bräuning-Demian, K. Carnes, S. Dreuil, V. Mergel, P. Richard, J. Ullrich, and H. Schmidt-Böcking, J. Phys. B **31**, 5149 (1998).
[4] H. Hasegawa, E. J. Takahashi, Y. Nabekawa, K. L. Ishikawa, and K. Midorikawa, Phys. Rev. A **71**, 023407 (2005).
[5] A. A. Sorokin, M. Wellhöfer, S. V. Bobashev, K. Tiedtke, and M. Richter, Phys. Rev. A **75**, 051402(R) (2007).
[6] J. Feist, S. Nagele, R. Pazourek, E. Persson, B. I. Schneider, L. A. Collins, and J. Burgdörfer, Phys. Rev. A **77**, 043420 (2008).
[7] J. Feist, R. Pazourek, S. Nagele, E. Persson, B. I. Schneider, L. A. Collins, and J. Burgdörfer, J. Phys. B **42**, 134014 (2009).
[8] A. Palacios, T. N. Rescigno, and C. W. McCurdy, Phys. Rev. A **77**, 032716 (2008).
[9] A. Palacios, T. N. Rescigno, and C. W. McCurdy, Phys. Rev. A **79**, 033402 (2009).
[10] A. Palacios, D. A. Horner, T. N. Rescigno, and C. W. McCurdy, J. Phys. B **43**, 194003 (2010).
[11] S. Chattopadhyay, C. Marante, B. I. Schneider, and L. Argenti, Phys. Rev. A **108**, 013114 (2023).
[12] X. Li *et al.*, Phys. Rev. Res. **4**, 013029 (2022).
[13] C. Cheng, L. J. Frasinski, G. Mogol, F. Allum, A. J. Howard, D. Rolles, P. H. Bucksbaum, M. Brouard, R. Forbes, and T. Weinacht, Phys. Rev. Lett. **130**, 093001 (2023).
[14] K. Motomura *et al.*, J. Phys. Chem. Lett. **6**, 2944 (2015).
[15] M. Kunitski, S. Zeller, J. Voigtsberger, A. Kalinin, L. P. H. Schmidt, M. Schöffler, A. Czasch, W. Schöllkopf, R. E. Grisenti, T. Jahnke, D. Blume, and R. Dörner, J. Phys. Conf. Ser. **635**, 112096 (2015).

[16] H. Ibrahim, B. Wales, S. Beaulieu, B. E. Schmidt, N. Thiré, E. P. Fowe, É. Bisson, C. T. Hebeisen, V. Wanie, M. Giguére, J.-C. Kieffer, M. Spanner, A. D. Bandrauk, J. Sanderson, M. S. Schuurman, and F. Légaré, Nat. Commun. **5**, 4422 (2014).
[17] S. Pathak, R. Obaid, S. Bhattacharyya, J. Bürger, X. Li, J. Tross, T. Severt, B. Davis, R. C. Bilodeau, C. A. Trallero-Herrero, A. Rudenko, N. Berrah, and D. Rolles, J. Phys. Chem. Lett. **11**, 10205 (2020).
[18] Y. H. Jiang *et al.*, Phys. Rev. A **81**, 051402(R) (2010).
[19] Y. H. Jiang *et al.*, Phys. Rev. A **81**, 021401(R) (2010).
[20] A. S. Kheifets and I. A. Ivanov, J. Phys. B **39**, 1731 (2006).
[21] J. Colgan, M. S. Pindzola, and F. Robicheaux, J. Phys. B **41**, 121002 (2008).
[22] F. Morales, F. Martín, D. A. Horner, T. N. Rescigno, and C. W. McCurdy, J. Phys. B **42**, 134013 (2009).
[23] X. Guan, K. Bartschat, and B. I. Schneider, Phys. Rev. A **82**, 041404(R) (2010).
[24] X. Guan, K. Bartschat, and B. I. Schneider, Phys. Rev. A **83**, 043403 (2011).
[25] X. Guan, K. Bartschat, B. I. Schneider, and L. Koesterke, Phys. Rev. A **88**, 043402 (2013).
[26] I. A. Ivanov and A. S. Kheifets, Phys. Rev. A **87**, 023414 (2013).
[27] X. Guan, K. Bartschat, B. I. Schneider, and L. Koesterke, Phys. Rev. A **90**, 043416 (2014).
[28] I. A. Ivanov and A. S. Kheifets, Phys. Rev. A **79**, 023409 (2009).
[29] W. Vanroose, F. Martín, T. N. Rescigno, and C. W. McCurdy, Science **310**, 1787 (2005).
[30] W. Vanroose, D. A. Horner, F. Martín, T. N. Rescigno, and C. W. McCurdy, Phys. Rev. A **74**, 052702 (2006).
[31] D. Jelovina, A full dimensional discrete variable representation of H2+ and H2 photoionization, Doctoral thesis, Universidad Autónoma de Madrid, 2017.
[32] D. Jelovina, J. Feist, F. Martín, and A. Palacios, Phys. Rev. A **95**, 043424 (2017).
[33] D. Jelovina, J. Feist, F. Martín, and A. Palacios, New J. Phys. **20**, 123004 (2018).
[34] A. Palacios, T. N. Rescigno, and C. W. McCurdy, Phys. Rev. Lett. **103**, 253001 (2009).
[35] M. Waitz *et al.*, Nat. Commun. **8**, 2266 (2017).
[36] I. Sánchez and F. Martín, J. Chem. Phys. **107**, 8391 (1997).
[37] A. Palacios, J. L. Sanz-Vicario, and F. Martín, J. Phys. B **48**, 242001 (2015).

End Matter

Appendix: Computational details—All the calculations presented in this Letter were computed using an FEM-DVR grid with 15 basis functions per finite element. The electronic coordinates are defined up to a maximum range of 200 a.u. with an exterior complex scaling of the coordinates at 160 a.u. For the angular expansion we employed a complete set of coupled spherical harmonics with angular momenta up to $l_{\max} = 6$. The nuclear coordinates are defined in a range up to 6 a.u., with nuclear motion restricted to the radial direction without accounting for rotations and only considering the interaction with linearly polarized light parallel to the nuclear axis. Although the implementation can account for all angular components, this would significantly increase the already high computational cost for double ionization and the laser parameters under study. We thus focus on understanding the mechanisms and dynamical electron-nuclear correlation effects, whose dependencies and trends can be generalized to other molecular orientations.

For the above-described dimensions of the basis set, the simulations required up to 21,120 processors distributed in 440 nodes. The number of processors needed is mostly dependent on memory storage per node. In other words, parallelization is a must due to the memory required to allocate the matrices and vectors, not due to computer waiting times. The time propagation is the computationally most expensive step and took around 10 h for a total propagation time of 2 fs. We are employing a custom short iterative Lanczos propagation algorithm, which we have checked to be numerically more stable and efficient for these large sparse matrices compared to Runge-Kutta and Crank-Nicolson propagators.

The evaluation of the ionization amplitudes is carried out with a direct projection [6,7] onto products of the one-electron continuum states of the H_2^+ ion [30], which are here computed explicitly including their dependence on the nuclear coordinates [31]. For the wavelengths under study, we can safely work within the dipole approximation to treat the laser-molecule interaction. The simulations presented here are obtained in velocity gauge, which provides faster numerical convergence with angular momentum. Nevertheless, in a few selected cases, we have checked that angular and energy-differential double ionization probabilities converge to the same values within the length gauge and are nearly undistinguishable from those obtained in the velocity gauge.